
Description of Sea-Ice Component of Coupled Ocean–Sea-Ice Model for the Earth Simulator (OIFES)

Nobumasa Komori^{1*}, Keiko Takahashi¹, Kenji Komine¹,
Tatsuo Motoi^{2†}, Xiangdong Zhang³ and Genki Sagawa^{1‡}

¹ The Earth Simulator Center, Japan Agency for Marine–Earth Science and Technology, Yokohama, Japan

² Frontier Research System for Global Change, Yokohama, Japan

³ International Arctic Research Center, University of Alaska, Fairbanks, Alaska, U.S.A.

(Received May 31, 2005; Revised manuscript accepted August 17, 2005)

Abstract In this report, sea-ice component of OIFES, Coupled Ocean–Sea-Ice Model for the Earth Simulator, is briefly described. It employs elastic–viscous–plastic rheology for dynamics considering massively parallel computation on the Earth Simulator, and simple zero-layer model for thermodynamics. Some early results are also presented.

Keywords: sea-ice model, elastic–viscous–plastic rheology, parallel computation

1. Introduction

Coupled Ocean–Sea-Ice Model for the Earth Simulator, named OIFES, is an extended version of OFES, Ocean General Circulation Model (GCM) for the Earth Simulator [1]. OFES is developed mainly to study the ocean surface circulations in tropical and subtropical regions and therefore the computational domain used by Masumoto et al. [1] excludes polar regions. OIFES contains a sea-ice model to be used for global ocean simulations including the Arctic and Antarctic regions and for coupled atmosphere–ocean simulations as an oceanic part of CFES, Coupled GCM for the Earth Simulator.

The sea-ice component of OIFES is implemented as a set of subroutines instead of an independent program from an ocean model. The ocean component of OIFES is almost identical to OFES, which is based on Modular Ocean Model version 3 (MOM3) [2] developed at Geophysical Fluid Dynamics Laboratory (GFDL). Therefore, the ocean component of OIFES is not touched on in this report.

The sea-ice model is based on the model developed at International Arctic Research Center (IARC) of University of Alaska [3], which is coupled with GFDL MOM2 [4] and employs dynamics with viscous–plastic (VP) rheology of Hibler [5] and zero-layer thermodynamics of Parkinson and Washington [6] with snow effects of

Oberhuber et al. [7]. Their coupled ocean–sea-ice model is used for regional study of the Arctic Ocean.

However, momentum equation of sea-ice with VP rheology is not suitable for massively parallel computation on the Earth Simulator, because it is usually solved implicitly and needs many iterations to get the solution of Poisson’s equation. Therefore, we have extended their sea-ice dynamics from VP rheology to elastic–viscous–plastic (EVP) rheology adopted from Hunke and Dukowicz [8], in which momentum equation of sea-ice is solved explicitly. We also modified the coordinate system from Cartesian coordinates to spherical coordinates following Hunke and Dukowicz [9] to cover the global ocean. In order to respond to the improvement in surface treatment of the ocean component from rigid-lid approximation (MOM2) to free-surface (MOM3), fresh water flux is adopted for boundary condition between sea-ice and ocean instead of salinity flux. Additionally, some modifications are applied to sea-ice thermodynamics for coupling with AFES, Atmospheric GCM for the Earth Simulator [10], and the source code is entirely parallelized using MPI (message passing interface). Incidentally, one may find the word “IARC” in some compile options described below, but note that many of them (such as `iarc_ice_evp`) are implemented within the Earth Simulator Center.

In this report, subscripts a , i , s , and w denote air

* **Corresponding author:** Dr. Nobumasa Komori, The Earth Simulator Center, Japan Agency for Marine–Earth Science and Technology, 3173–25 Showa-machi, Kanazawa, Yokohama, Kanagawa 236-0001, E-mail: komori@jamstec.go.jp

† Now at Meteorological Research Institute, Japan Meteorological Agency, Tsukuba, Japan

‡ Now at Department of Environmental and Ocean Engineering, University of Tokyo, Tokyo, Japan

(atmosphere), sea-ice, snow, and seawater (ocean), respectively, and superscript *eff* means an “effective” variable, which is multiplied by sea-ice concentration or, in other words, averaged within a model grid. Subroutine names are written in *italic* and option names are expressed in sans serif.

2. Fundamentals

2.1 Model Variables, Constants, and Namelist Parameters

Sea-ice is assumed to exist over sea surface with the thickness of h_i and the concentration of A_i , and to move with the velocity $\mathbf{u}_i = (u_i, v_i)$. In addition, snow lies on sea-ice with the depth of h_s . Figure 1 shows a schematic of sea-ice model. Actually, effective sea-ice thickness $h_i^{eff} = A_i h_i$ and effective snow depth $h_s^{eff} = A_i h_s$ are prognostic variables instead of h_i and h_s , respectively. We call A_i , h_i^{eff} , and h_s^{eff} “tracers” in this report for convenience.

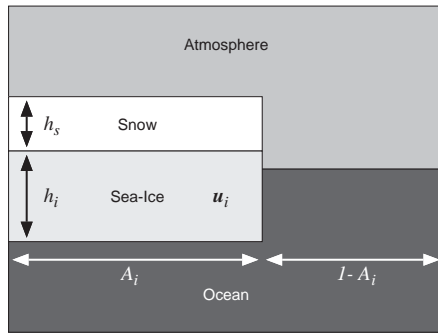


Fig. 1 Schematics of sea-ice model.

Table 1 Prognostic variables in OIFES.

Symbol	Description	Unit
A_i	sea-ice concentration	[-]
h_i^{eff}	effective sea-ice thickness	[m]
h_s^{eff}	effective snow depth	[m]
u_i	zonal component of sea-ice velocity	[m s ⁻¹]
v_i	meridional component of sea-ice velocity	[m s ⁻¹]

Model variables, constants, and namelist parameters are summarized in Tables 1, 2, and 3, respectively.

2.2 Coordinate System

The sea-ice component of OIFES employs a 2-dimensional spherical coordinate system, so the position is

Table 2 Constants used in OIFES.

Symbol	Description	Value
a	radius of the earth	$6,371 \times 10^3$ [m]
c_{pa}	specific heat of air	1005.0 [J kg ⁻¹ K ⁻¹]
c_{pw}	specific heat of seawater	4218.0 [J kg ⁻¹ K ⁻¹]
g	acceleration due to gravity	9.806 [m s ⁻²]
k_i	thermal conductivity of ice	2.0344 [W m ⁻¹ K ⁻¹]
k_s	thermal conductivity of snow	0.3098 [W m ⁻¹ K ⁻¹]
L_{melt}	latent heat of fusion	3.4×10^5 [J kg ⁻¹]
L_{vap}	latent heat of vaporization	2.5×10^6 [J kg ⁻¹]
T_0	freezing point of fresh water	273.15 [K]
T_w^{frz}	freezing point of seawater *	271.20 [K]
T_i^{melt}	melting point of sea-ice	273.05 [K]
T_s^{melt}	melting point of snow	273.15 [K]
α_i^{dry}	albedo of dry sea-ice	0.60
α_i^{wet}	albedo of wet sea-ice	0.50
α_s^{dry}	albedo of dry snow	0.84
α_s^{wet}	albedo of wet snow	0.70
α_w	albedo of seawater	0.10
γ	adiabatic lapse rate	0.01 [K m ⁻¹]
ϵ_i	sea-ice emissivity	0.97
ϵ_s	snow emissivity	0.99
ϵ_w	seawater emissivity	0.97
κ	von Kármán's constant	0.4
ρ_a	air density	1.2 [kg m ⁻³]
ρ_f	fresh water density	1000 [kg m ⁻³]
ρ_i	sea-ice density	920 [kg m ⁻³]
ρ_s	snow density	330 [kg m ⁻³]
ρ_w	seawater density	1026 [kg m ⁻³]
σ	Stefan-Boltzman constant	5.67×10^{-8} [W m ⁻² K ⁻¹]

*When the option `variable_ticb` is enabled, T_w^{frz} becomes a diagnostic variable.

Table 3 Namelist parameters in OIFES. Test values are used for test run described in Section 8.

Symbol	Description	Default Value	Test Value
A_{i_min}	minimum sea-ice concentration	0.15	0.01
C_t	bulk transfer coefficient	9.65×10^{-6} [m s ⁻¹]	9.65×10^{-5} [m s ⁻¹]
d_1	diffusivity for harmonic-type operator	0.004 [m s ⁻¹]	0.004 [m s ⁻¹]
d_2	diffusivity for biharmonic-type operator	0.004 [m s ⁻¹]	0.004 [m s ⁻¹]
$h_{i_min}^{eff}$	minimum sea-ice thickness	0.01 [m]	0.01 [m]
N_{evp}	number of elastic subcycle	72	10
P	coefficient for sea-ice pressure	2.75×10^4 [Pa]	10.0×10^4 [Pa]
$\rho_w C_{Dw}$	seawater density \times bulk drag coefficient	5.5 [kg m ⁻³]	5.5 [kg m ⁻³]

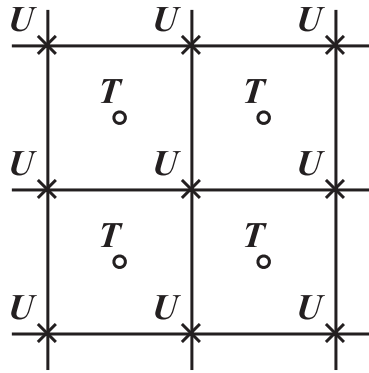


Fig. 2 Spatial arrangement of variables. The letters T and U refer tracer point and velocity point, respectively. A_i , h_i^{eff} , and h_s^{eff} are defined at tracer points and u_i and v_i are at velocity points.

expressed by longitude λ and latitude ϕ . The Arakawa B-grid is used for spatial discretization, and A_i , h_i^{eff} , and h_s^{eff} are arranged to so-called tracer points and u_i and v_i are to velocity points (Fig. 2). The grid spacing is set to the same value as in the ocean component in subroutine *setice*.

2.3 Governing Equations

Momentum equation of sea-ice is expressed as follows¹ [5, Eq. (1)]:

$$m_i^{eff} \frac{\partial \mathbf{u}_i}{\partial t} = -m_i^{eff} f \mathbf{k} \times \mathbf{u}_i + \boldsymbol{\tau}_{ai}^{eff} + \boldsymbol{\tau}_{iw}^{eff} - m_i^{eff} g \nabla h_w + \mathbf{F}, \quad (1)$$

where $m_i^{eff} = \rho_i h_i^{eff} + \rho_s h_s^{eff}$ is total mass of sea-ice and snow per unit area, ρ_i sea-ice density, ρ_s snow density, f the Coriolis parameter, \mathbf{k} a unit vector normal to the surface, $\boldsymbol{\tau}_{ai}^{eff} = A_i \boldsymbol{\tau}_{ai}$ effective wind stress, $\boldsymbol{\tau}_{iw}^{eff} = A_i \boldsymbol{\tau}_{iw}$ effective ocean stress, g acceleration due to gravity, h_w sea surface height, and \mathbf{F} internal ice force. Note that sea surface height h_w is now a prognostic variable calculated in the ocean component of OIFES, so ∇h_w is evaluated directly from h_w rather than from the geostrophic ocean current. Detail about internal ice force \mathbf{F} is described in section 4.1.

For sea-ice concentration A_i , effective sea-ice thickness h_i^{eff} , and effective snow depth h_s^{eff} , tracer equations are given as follows [5, Eqs. (13) and (14)]:

$$\frac{\partial A_i}{\partial t} = -\mathcal{L}(A_i) + \mathcal{D}(A_i) + F_A, \quad (2)$$

$$\frac{\partial h_i^{eff}}{\partial t} = -\mathcal{L}(h_i^{eff}) + \mathcal{D}(h_i^{eff}) + F_i^{eff}, \quad (3)$$

$$\frac{\partial h_s^{eff}}{\partial t} = -\mathcal{L}(h_s^{eff}) + \mathcal{D}(h_s^{eff}) + F_s^{eff}, \quad (4)$$

where \mathcal{L} and \mathcal{D} represent advection and diffusion operators, respectively (see section 4.2), and F_A , F_i^{eff} , and F_s^{eff} are source terms determined from thermodynamic process described in section 5.

3. Connection with Other Components

3.1 Atmosphere

In order to drive OIFES, wind stress $\boldsymbol{\tau}_a$, downward short- and long-wave radiation fluxes, $R_{SW} \downarrow$ and $R_{LW} \downarrow$, sensible and latent heat fluxes, $H_{sen} \downarrow$ and $H_{lat} \downarrow$, rainfall W_{rain} , snowfall W_{snow} , river runoff W_{river} , and sea-ice/snow surface temperature T_{sfc} are needed. In the case of stand-alone simulation, some of them are calculated in OIFES using surface atmospheric data, while in the case of coupled simulation, all of them are calculated in AFES.

If the option *iarc_flg* is enabled, forcing data dependent on ocean/sea-ice variables (sea-ice/snow surface temperature T_{sfc} , sensible heat flux $H_{sen} \downarrow$, and latent heat flux $H_{lat} \downarrow$) are calculated within OIFES using bulk formula from surface air temperature T_a , surface specific humidity q_a , surface wind speed $\|\mathbf{V}_a\|$, and surface air pressure p_{sfc} . Additionally, rainfall W_{rain} and snowfall W_{snow} are parameterized from precipitation W_{prcp} and surface air temperature T_a . In detail, see section 5. Other forcing data are provided from some data sets such as NCEP/NCAR reanalysis.

When the option *cfes* is enabled, OIFES is coupled with AFES and all forcing data are provided from the atmospheric component. In this case, following variables are transferred from the ocean/sea-ice component to the atmospheric component in order to calculate surface fluxes: ocean surface temperature T_w , sea-ice concentration A_i , effective sea-ice thickness h_i^{eff} , effective snow depth h_s^{eff} , and freezing point of seawater T_w^{fz} (only if the option *variable_ticb* is enabled).

3.2 Ocean

From the ocean component, temperature T_w , salinity S_w , and velocity $\mathbf{u}_w = (u_w, v_w)$ of the top level and sea surface height h_w are input to the sea-ice component.

If the option *variable_ticb* is enabled, freezing point of seawater, T_w^{fz} , is evaluated as a linear function² of surface salinity S_w as

$$T_w^{fz} = T_0 - \mu S_w, \quad (5)$$

where T_0 is freezing point of freshwater and $\mu = 0.0543$

¹ Advection term is neglected in the current version of OIFES.

² This should be extended to a nonlinear function of S_w in future.

K psu⁻¹ [11]. Otherwise, T_w^{frz} is taken as constant value (271.2 K).

After the sea-ice variables are updated, resulting momentum flux $\boldsymbol{\tau}_{surf}$, heat flux Q_{surf} , and fresh water flux W_{surf} are provided as surface boundary conditions for the ocean component (see section 6).

4 Dynamics

Sea-ice dynamics is a two-dimensional (horizontal) process and consists of momentum equation (section 4.1) and tracer advection/diffusion (section 4.2).

4.1 Momentum Equation

Again, momentum equation of sea-ice is expressed as follows:

$$m_i^{eff} \frac{\partial u_i}{\partial t} = +m_i^{eff} f v_i + \tau_{ai,\lambda}^{eff} + \tau_{iw,\lambda}^{eff} - m_i^{eff} g \frac{1}{a \cos \phi} \frac{\partial h_w}{\partial \lambda} + F_\lambda. \quad (1a)$$

$$m_i^{eff} \frac{\partial v_i}{\partial t} = -m_i^{eff} f u_i + \tau_{ai,\phi}^{eff} + \tau_{iw,\phi}^{eff} - m_i^{eff} g \frac{1}{a} \frac{\partial h_w}{\partial \phi} + F_\phi. \quad (1b)$$

Given the ocean surface velocity \mathbf{u}_w , ocean stress $\boldsymbol{\tau}_{iw}$ is expressed as a function of sea-ice velocity \mathbf{u}_i as [5, Eq. (2)]:

$$\boldsymbol{\tau}_{iw} = \rho_w C_{Dw} \|\mathbf{u}_w - \mathbf{u}_i\| \left[(\mathbf{u}_w - \mathbf{u}_i) \cos \theta + \mathbf{k} \times (\mathbf{u}_w - \mathbf{u}_i) \sin \theta \right], \quad (6)$$

where ρ_w is seawater density, C_{Dw} the bulk drag coefficient, θ water turning angle. Note that previous studies [5, 8] used the geostrophic ocean current \mathbf{U}_w of the interior region (rather than \mathbf{u}_w) and θ was set to be 25°, but our OGCM usually has enough vertical resolution of several meters at surface and therefore we set θ to be zero. The ocean stress term and the Coriolis term are treated implicitly.

Internal ice force $\mathbf{F} = (F_\lambda, F_\phi)$ is calculated as the divergence of stress tensor $\boldsymbol{\sigma}$ [12]:

$$F_\lambda = \frac{1}{a \cos \phi} \frac{\partial \sigma_{\lambda\lambda}}{\partial \lambda} + \frac{1}{a} \frac{\partial \sigma_{\lambda\phi}}{\partial \phi} - \frac{2\sigma_{\lambda\phi} \tan \phi}{a}, \quad (7a)$$

$$F_\phi = \frac{1}{a \cos \phi} \frac{\partial \sigma_{\lambda\phi}}{\partial \lambda} + \frac{1}{a} \frac{\partial \sigma_{\phi\phi}}{\partial \phi} + \frac{(\sigma_{\lambda\lambda} - \sigma_{\phi\phi}) \tan \phi}{a}. \quad (7b)$$

Stress tensor $\boldsymbol{\sigma}$ is related to strain rate $\dot{\boldsymbol{\epsilon}}$ and pressure P via a constitutive law, which depends on the treatment of sea-ice rheology (see subsection 4.1.1 for VP model and 4.1.2 for EVP model).

Strain rate $\dot{\boldsymbol{\epsilon}}$ is expressed by means of sea-ice velocity \mathbf{u}_i as follows [12]:

$$\dot{\epsilon}_{\lambda\lambda} = \frac{1}{a \cos \phi} \frac{\partial u_i}{\partial \lambda} - \frac{v_i \tan \phi}{a}, \quad (8a)$$

$$\dot{\epsilon}_{\phi\phi} = \frac{1}{a} \frac{\partial v_i}{\partial \phi}, \quad (8b)$$

$$\dot{\epsilon}_{\lambda\phi} = \frac{1}{2} \left(\frac{1}{a} \frac{\partial u_i}{\partial \phi} + \frac{u_i \tan \phi}{a} + \frac{1}{a \cos \phi} \frac{\partial v_i}{\partial \lambda} \right), \quad (8c)$$

The pressure P , which is a measure of sea-ice strength, is parameterized as a function of sea-ice thickness and concentration as follows [5, Eq. (17)]:

$$P = P^* h_i^{eff} \exp[-C(1 - A_i)], \quad (9)$$

where P^* (a namelist parameter) and $C = 20$ are empirical constants. Nonlinear shear viscosity $\eta = \eta(\dot{\boldsymbol{\epsilon}}, P)$ and nonlinear bulk viscosity $\zeta = \zeta(\dot{\boldsymbol{\epsilon}}, P)$, which are used to calculate stress tensor $\boldsymbol{\sigma}$, are parameterized as [5]:

$$\zeta = P/2\Delta, \quad (10)$$

$$\eta = \zeta/e^2, \quad (11)$$

where

$$\Delta = \left[\left(\dot{\epsilon}_{\lambda\lambda}^2 + \dot{\epsilon}_{\phi\phi}^2 \right) (1 + e^{-2}) + 4e^{-2} \dot{\epsilon}_{\lambda\phi}^2 + 2\dot{\epsilon}_{\lambda\lambda} \dot{\epsilon}_{\phi\phi} (1 - e^{-2}) \right]^{1/2} \quad (12)$$

and e is the ratio of principal axes of the ellipse and equal to 2. In order to avoid the viscosities become infinite in the limit of zero strain rate, we set upper bounds of ζ and η as

$$\zeta_{max} = (2.5 \times 10^8) P, \quad (13)$$

$$\eta_{max} = \zeta_{max}/e^2. \quad (14)$$

We also set lower bound as $\zeta_{min} = 4.0 \times 10^8$ kg s⁻¹, and if $\zeta_{max} < \zeta_{min}$ then $\zeta = \zeta_{min}$.

4.1.1 Viscous–Plastic Model

If the option `iarc_ice_hib` is enabled, VP type constitutive law [5] is adopted.

In this case, stress tensor $\boldsymbol{\sigma}$ is given by

$$\sigma_{\lambda\lambda} = (\zeta + \eta) \dot{\epsilon}_{\lambda\lambda} + (\zeta - \eta) \dot{\epsilon}_{\phi\phi} - P/2, \quad (15a)$$

$$\sigma_{\phi\phi} = (\zeta - \eta) \dot{\epsilon}_{\lambda\lambda} + (\zeta + \eta) \dot{\epsilon}_{\phi\phi} - P/2, \quad (15b)$$

$$\sigma_{\lambda\phi} = 2\eta \dot{\epsilon}_{\lambda\phi}. \quad (15c)$$

Thus, stress tensor $\boldsymbol{\sigma}$ is diagnosed from sea-ice velocity \mathbf{u}_i through strain rate $\dot{\boldsymbol{\epsilon}}$ using Eqs. (8) and (15), and momentum equation (1) is solved iteratively using the following relationship:

$$\begin{aligned} F_\lambda = & \frac{1}{a \cos \phi} \frac{\partial}{\partial \lambda} \left[(\zeta + \eta) \left(\frac{1}{a \cos \phi} \frac{\partial u_i}{\partial \lambda} - \frac{v_i \tan \phi}{a} \right) \right. \\ & \left. + (\zeta - \eta) \left(\frac{1}{a} \frac{\partial v_i}{\partial \phi} \right) - \frac{P}{2} \right] \\ & + \frac{1}{a} \frac{\partial}{\partial \phi} \left[\eta \left(\frac{1}{a} \frac{\partial u_i}{\partial \phi} + \frac{u_i \tan \phi}{a} + \frac{1}{a \cos \phi} \frac{\partial v_i}{\partial \lambda} \right) \right] \\ & - \frac{2 \tan \phi}{a} \left[\eta \left(\frac{1}{a} \frac{\partial u_i}{\partial \phi} + \frac{u_i \tan \phi}{a} + \frac{1}{a \cos \phi} \frac{\partial v_i}{\partial \lambda} \right) \right], \quad (16a) \end{aligned}$$

$$\begin{aligned} F_\phi = & \frac{1}{a \cos \phi} \frac{\partial}{\partial \lambda} \left[\eta \left(\frac{1}{a} \frac{\partial u_i}{\partial \phi} + \frac{u_i \tan \phi}{a} \right. \right. \\ & \left. \left. + \frac{1}{a \cos \phi} \frac{\partial v_i}{\partial \lambda} \right) \right] \\ & + \frac{1}{a} \frac{\partial}{\partial \phi} \left[(\zeta - \eta) \left(\frac{1}{a \cos \phi} \frac{\partial u_i}{\partial \lambda} - \frac{v_i \tan \phi}{a} \right) \right. \\ & \left. + (\zeta + \eta) \left(\frac{1}{a} \frac{\partial v_i}{\partial \phi} \right) - \frac{P}{2} \right] \\ & + \frac{2 \tan \phi}{a} \left[\eta \left(\frac{1}{a \cos \phi} \frac{\partial u_i}{\partial \lambda} - \frac{v_i \tan \phi}{a} - \frac{1}{a} \frac{\partial v_i}{\partial \phi} \right) \right]. \quad (16b) \end{aligned}$$

4.1.2 Elastic–Viscous–Plastic Model

If the option `iarc_ice_evp` is enabled, EVP type constitutive law [8] is adopted.

Constitutive law of VP model, Eq. (15), can be rewritten in the form:

$$\frac{\zeta + \eta}{4\zeta\eta} \sigma_{\lambda\lambda} - \frac{\zeta - \eta}{4\zeta\eta} \sigma_{\phi\phi} + \frac{P}{4\zeta} = \dot{\epsilon}_{\lambda\lambda}, \quad (17a)$$

$$-\frac{\zeta - \eta}{4\zeta\eta} \sigma_{\lambda\lambda} + \frac{\zeta + \eta}{4\zeta\eta} \sigma_{\phi\phi} + \frac{P}{4\zeta} = \dot{\epsilon}_{\phi\phi}, \quad (17b)$$

$$\frac{1}{2\eta} \sigma_{\lambda\phi} = \dot{\epsilon}_{\lambda\phi}. \quad (17c)$$

By introducing “pseudo” elastic contribution to the con-

stitutive law, we obtain

$$\frac{1}{E} \frac{\partial \sigma_{\lambda\lambda}}{\partial t} + \frac{\zeta + \eta}{4\zeta\eta} \sigma_{\lambda\lambda} - \frac{\zeta - \eta}{4\zeta\eta} \sigma_{\phi\phi} + \frac{P}{4\zeta} = \dot{\epsilon}_{\lambda\lambda}, \quad (18a)$$

$$\frac{1}{E} \frac{\partial \sigma_{\phi\phi}}{\partial t} - \frac{\zeta - \eta}{4\zeta\eta} \sigma_{\lambda\lambda} + \frac{\zeta + \eta}{4\zeta\eta} \sigma_{\phi\phi} + \frac{P}{4\zeta} = \dot{\epsilon}_{\phi\phi}, \quad (18b)$$

$$\frac{1}{E} \frac{\partial \sigma_{\lambda\phi}}{\partial t} + \frac{1}{2\eta} \sigma_{\lambda\phi} = \dot{\epsilon}_{\lambda\phi}, \quad (18c)$$

where E corresponds to Young’s modulus. The parameter E is determined to satisfy the CFL condition as:

$$E = \frac{2E_0 m_i^{eff}}{(\Delta t_{evp})^2} \times \min \left[(a \cos \phi \Delta \lambda)^2, (a \Delta \phi)^2 \right], \quad (19)$$

where E_0 is a constant (0.25). Thus, temporal changes of stress tensor $\boldsymbol{\sigma}$ and sea-ice velocity \mathbf{u}_i are solved simultaneously using Eqs. (1), (7), (8), and (18) with an elastic subcycling time step $\Delta t_{evp} = \Delta t / N_{evp}$, where N_{evp} is a number of elastic subcycle (a namelist parameter).

4.2 Tracer Advection and Diffusion

In the subroutine `advdif`, temporal changes of tracers due to advection and diffusion are calculated.

Advection operator \mathcal{L} is given as follows:

$$\begin{aligned} \mathcal{L}(\alpha) &= \nabla \cdot (\mathbf{u}_i \alpha) \\ &= \frac{1}{a \cos \phi} \frac{\partial}{\partial \lambda} (u_i \alpha) + \frac{1}{a \cos \phi} \frac{\partial}{\partial \phi} (v_i \alpha \cos \phi), \quad (20) \end{aligned}$$

where α corresponds to A_i , h_i^{eff} , or h_s^{eff} and \mathbf{u}_i is sea-ice velocity. Simple second-order finite volume method is implemented as advection scheme.

When the option `iarc_ice_biharmonic` is NOT enabled, harmonic-type horizontal diffusion operator is used:

$$\begin{aligned} \mathcal{D}(\alpha) &= \nabla \cdot (D_1 \nabla \alpha) \\ &= \frac{1}{a \cos \phi} \frac{\partial}{\partial \lambda} \left(\frac{D_1}{a \cos \phi} \frac{\partial \alpha}{\partial \lambda} \right) \\ &+ \frac{1}{a \cos \phi} \frac{\partial}{\partial \phi} \left(\cos \phi \frac{D_1}{a} \frac{\partial \alpha}{\partial \phi} \right), \quad (21) \end{aligned}$$

For default setting, diffusivity D_1 is

$$D_1 = d_1 (a \Delta \lambda),$$

while in the case that the option `iarc_ice_am_cosine` is enabled,

$$D_1 = d_1 (a \Delta \lambda \cos \phi),$$

where d_1 is a namelist parameter.

When the option `iarc_ice_biharmonic` is enabled, har-

monic + biharmonic-type horizontal diffusion operator is used:

$$\mathcal{D}(\alpha) = \nabla \cdot (D_1 \nabla \alpha) - \nabla \cdot (D_2 \nabla^3 \alpha). \quad (22)$$

For default setting, diffusivities D_1 and D_2 are

$$D_1 = d_1 (a\Delta\lambda), \quad D_2 = d_2 (a\Delta\lambda)^3,$$

while in the case that the option `iarc_ice_am_cosine` is enabled,

$$D_1 = d_1 (a\Delta\lambda \cos \phi), \quad D_2 = d_2 (a\Delta\lambda \cos \phi)^3,$$

where d_1 and d_2 are namelist parameters.

4.3 Polar Filter

If the options `iarc_ice_filter` and `firfil` are enabled, a finite impulse response filter is applied to sea-ice velocity \mathbf{u}_i at each elastic subcycle in a similar way to that applied to ocean velocity in order to relax the time step constraint imposed by convergence of meridians. In detail, refer to MOM3 manual [2, Chapter 27]. The same reference latitudes (the filtering is applied poleward of these latitudes) as set for the oceanic variables are used.

5 Thermodynamics

Thermodynamic model of sea-ice is based on that proposed by Parkinson and Washington [6], which is a Semtner-type [13] zero-layer model. Open ocean (or lead) and sea-ice region within a model grid are treated separately (sections 5.1 and 5.2, respectively) and resulting growth rates of sea-ice are combined using sea-ice concentration (section 5.3). Figure 3 shows a schematic diagram of our thermodynamic model. Note that sea-ice thermodynamics is a one-dimensional (vertical) process.

5.1 Open Ocean

5.1.1 Surface Fluxes

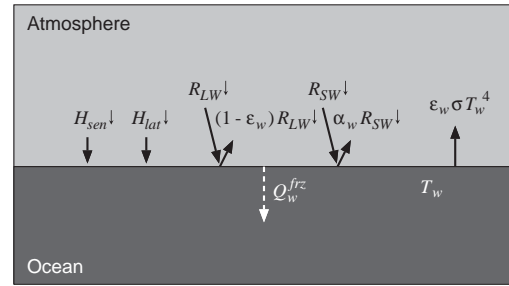
When the option `iarc_flg` is enabled, sensible and latent heat fluxes, $H_{sen} \downarrow$ and $H_{lat} \downarrow$, are evaluated using surface air temperature T_a , surface specific humidity q_a , surface wind speed $\|\mathbf{V}_a\|$, and surface air pressure p_{sfc} in subroutine `asflx` following procedures and coefficients of Large and Pond [14, 15].

Using bulk formulae with bulk transfer coefficients, C_H and C_E , turbulent heat fluxes are expressed as:

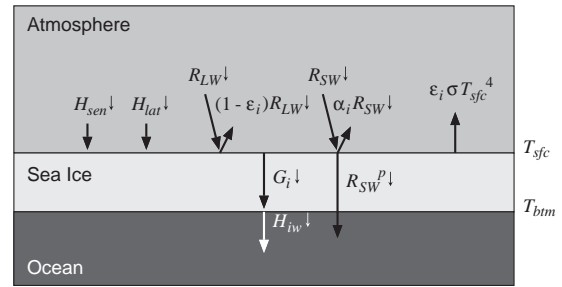
$$H_{sen} \downarrow = \rho_a c_{pa} C_H \|\mathbf{V}_a\| \Delta \theta, \quad (23)$$

$$H_{lat} \downarrow = \rho_a L_{vap} C_E \|\mathbf{V}_a\| \Delta q, \quad (24)$$

(a) open ocean (lead)



(b) snow-free sea-ice



(c) snow-covered sea-ice

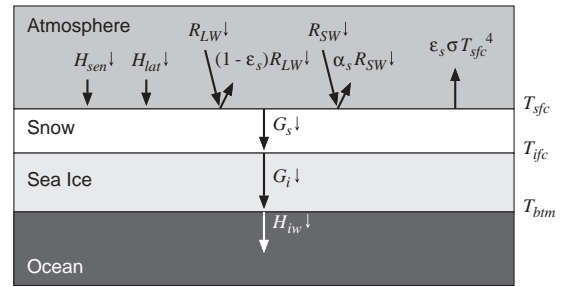


Fig. 3 Schematic diagrams of the energy fluxes involves for (a) open ocean, (b) snow-free sea-ice, and (c) snow-covered sea-ice. Adapted from Parkinson and Washington [6].

where ρ_a is air density, c_{pa} specific heat of air, and L_{vap} latent heat of vaporization. Potential temperature difference $\Delta\theta$ and specific humidity difference Δq are given as:

$$\Delta \theta = T_a + \gamma z_T - T_w, \quad (25)$$

$$\Delta q = q_a - q_{sfc}, \quad (26)$$

where γ is adiabatic lapse rate and $z_T = 2$ m observed height of T_a . Surface specific humidity q_{sfc} is calculated as:

$$q_{sfc} = 0.98 \times \frac{0.622 \times e_s}{p_{sfc} - 0.378 \times e_s}, \quad (27)$$

where the factor 0.98 is for seawater correction and e_s is saturation vapor pressure:

$$e_s = 6.11 \times 10^2 \exp\left(17.269 \times \frac{T_w - T_0}{T_w - T_0 + 237.3}\right). \quad (28)$$

Bulk coefficients, $C_D = c_D^2$, $C_H = c_H c_D$, and $C_E = c_E c_D$, are estimated iteratively as follows. Turbulent scales of velocity u^* , temperature T^* , and humidity q^* are evaluated by means of c_D , c_H , and c_E as:

$$u^* = c_D \|V_a\|, \quad (29)$$

$$T^* = c_H \Delta \theta, \quad (30)$$

$$q^* = c_E \Delta q, \quad (31)$$

and inverse of Monin-Obukhov length:

$$L^{-1} = \frac{\kappa g}{u^{*2}} \left(\frac{T^*}{T_v} + \frac{q^*}{1/0.606 + q_a} \right), \quad (32)$$

where κ is von Kármán's constant, g acceleration due to gravity, and T_v virtual temperature:

$$T_v = (1 + 0.606 \times q_a) T_a. \quad (33)$$

In turn, bulk coefficients are

$$c_D = \frac{c_{DN}}{1 + \kappa^{-1} c_{DN} [\ln(z_u/z_0) - \psi_u(z_u/L)]}, \quad (34)$$

$$c_H = \frac{c_{HN}}{1 + \kappa^{-1} c_{HN} [\ln(z_T/z_0) - \psi_T(z_T/L)]}, \quad (35)$$

$$c_E = \frac{c_{EN}}{1 + \kappa^{-1} c_{EN} [\ln(z_q/z_0) - \psi_q(z_q/L)]}, \quad (36)$$

where $z_u = 10$ m and $z_q = 2$ m are observed heights of $\|V_a\|$ and q_a , respectively, and $z_0 = 10$ m is a reference height. Bulk coefficients at z_0 with neutral stability, c_{DN} , c_{HN} , and c_{EN} , are given as:

$$c_{DN} = (0.0027 \times \|V_a\|^{-1} + 0.000142 + 0.0000764 \times \|V_a\|^{1/2}), \quad (37)$$

$$c_{HN} = \begin{cases} 0.0180 & \text{stable} \\ 0.0327 & \text{unstable} \end{cases} \quad (38)$$

$$c_{EN} = 0.0346, \quad (39)$$

and stability functions, ψ_u , ψ_T , and ψ_q , are

$$\psi_u(z/L) = \begin{cases} -5z/L & \text{stable} \\ 2 \ln [(1+X)/2] + \ln [(1+X^2)/2] & \\ -2 \tan^{-1} X + \pi/2 & \text{unstable} \end{cases} \quad (40)$$

$$\psi_T(z/L) = \psi_q(z/L) = \begin{cases} -5z/L & \text{stable} \\ 2 \ln [(1+X^2)/2] & \text{unstable} \end{cases} \quad (41)$$

with $X = (1 - 16 z/L)^{1/4}$ where ‘‘stable’’ means the case that z/L is positive. This procedure is iterated twice from the first guess $c_D = c_{DN}$, $c_H = c_{HN}$, and $c_E = c_{EN}$.

5.1.2 Formation Rate of Sea-Ice

Ocean surface heat flux Q_w is defined as:

$$Q_w = H_{lat} \downarrow + H_{sen} \downarrow + \epsilon_w R_{LW} \downarrow + (1 - \alpha_w) R_{SW} \downarrow - \epsilon_w R_w \uparrow, \quad (42)$$

where $H_{lat} \downarrow$ is latent heat flux, $H_{sen} \downarrow$ sensible heat flux, $R_{LW} \downarrow$ downward long-wave radiation flux, $R_{SW} \downarrow$ downward short-wave radiation flux, $R_w \uparrow$ upward long-wave radiation flux, ϵ_w seawater emissivity, and α_w seawater albedo (Fig. 3a). Upward long-wave radiation $R_w \uparrow$ is expressed by means of ocean surface temperature T_w as:

$$R_w \uparrow = \sigma T_w^4, \quad (43)$$

where σ is Stefan-Boltzman constant.

Here we evaluate Q_w^{frz} as

$$Q_w^{frz} = \rho_w c_{pw} \frac{\Delta z_w}{\Delta t} (T_w^{frz} - T_w), \quad (44)$$

where ρ_w is seawater density, c_{pw} specific heat of seawater, Δz_w the thickness of the top level of the ocean component including free surface, Δt time step, T_w^{frz} freezing point of seawater, and T_w ocean temperature of the top level. Q_w^{frz} is a negative heat flux necessary for water column with temperature T_w and thickness Δz_w to be frozen within a time Δt .

If ocean surface heat flux Q_w is greater than Q_w^{frz} , no sea-ice is formed and Q_w itself is used as a thermal boundary condition for the ocean component, Q_{aw} . When Q_w is less than Q_w^{frz} , their difference is utilized for sea-ice formation and in this case $Q_{aw} = Q_w^{frz}$. That is, formation rate of sea-ice, F_w , and residual heat flux into the ocean, Q_{aw} , are expressed as:

$$F_w = \max \left(0, \frac{Q_w^{frz} - Q_w}{\rho_i L_{mlt}} \right), \quad (45)$$

$$Q_{aw} = \max (Q_w, Q_w^{frz}), \quad (46)$$

where ρ_i is sea-ice density and L_{mlt} latent heat of fusion.

5.2 Sea-Ice Region

5.2.1 Surface Fluxes

Sea-ice/snow surface heat flux $Q_{sfc} \downarrow$ is defined as:

$$Q_{sfc} \downarrow = H_{lat} \downarrow + H_{sen} \downarrow + \epsilon_{sfc} R_{LW} \downarrow + (1 - \alpha_{sfc}) R_{SW} \downarrow - \epsilon_{sfc} R_{sfc} \uparrow, \quad (47)$$

where $H_{lat} \downarrow$ is latent heat flux, $H_{sen} \downarrow$ sensible heat flux, $R_{LW} \downarrow$ downward long-wave radiation flux, $R_{SW} \downarrow$ downward short-wave radiation flux, $R_{sfc} \uparrow$ upward long-wave radiation flux, ϵ_{sfc} surface emissivity, and α_{sfc} surface albedo. Upward long-wave radiation $R_{sfc} \uparrow$ is expressed as a function of surface temperature T_{sfc} as:

$$R_{sfc} \uparrow = \sigma T_{sfc}^4, \quad (48)$$

where σ is Stefan-Boltzman constant.

When sea-ice is not covered with snow ($h_s = 0$), surface emissivity ϵ_{sfc} is equal to sea-ice emissivity ϵ_i and surface albedo α_{sfc} is expressed with distinction between wet (melting) and dry ices as follows:

$$\alpha_{sfc} = \begin{cases} \alpha_i^{wet} & (T_{sfc} > T_i^{melt} - 0.001) \\ \alpha_i^{dry} & (T_{sfc} \leq T_i^{melt} - 0.001) \end{cases} \quad (49)$$

where T_i^{melt} is melting point of sea-ice. Otherwise ($h_s > 0$), surface emissivity ϵ_{sfc} is equal to snow emissivity ϵ_s and surface albedo α_{sfc} is expressed with distinction between wet (melting) and dry snows as follows:

$$\alpha_{sfc} = \begin{cases} \alpha_s^{wet} & (T_{sfc} > T_s^{melt} - 0.001) \\ \alpha_s^{dry} & (T_{sfc} \leq T_s^{melt} - 0.001) \end{cases} \quad (50)$$

where T_s^{melt} is melting point of snow.

When the option `iarc_flg` is enabled, sensible and latent heat fluxes, $H_{sen} \downarrow$ and $H_{lat} \downarrow$, are evaluated as a function of sea-ice/snow surface temperature T_{sfc} using surface air temperature T_a , surface specific humidity q_a , and surface wind speed $\|V_d\|$ in subroutine `budgets` as follows:

$$H_{sen} \downarrow = \rho_a c_{pa} C_H \|V_d\| (T_a - T_{sfc}), \quad (51)$$

$$H_{lat} \downarrow = \rho_a L_{sub} C_E \|V_d\| (q_a - q_{sfc}), \quad (52)$$

where ρ_a is air density, c_{pa} specific heat of air, $L_{sub} = L_{melt} + L_{vap}$ latent heat of sublimation, and C_H , C_E bulk transfer coefficients (constants). Saturated specific humidity q_{sfc} is calculated as:

$$q_{sfc} = \frac{0.622}{p_0} \times 6.11 \times 10^2 \times \exp\left(21.8746 \times \frac{T_{sfc} - T_0}{T_{sfc} - T_0 + 265.5}\right), \quad (53)$$

where $p_0 = 1013 \times 10^2$ Pa is a reference air pressure. Variations of sensible and latent heat fluxes with respect to surface temperature are expressed as:

$$\frac{\partial H_{sen} \downarrow}{\partial T_{sfc}} = -\rho_a c_{pa} C_H \|V_d\|, \quad (54)$$

$$\frac{\partial H_{lat} \downarrow}{\partial T_{sfc}} = -\rho_a L_{sub} C_E \|V_d\| q_{sfc} \frac{21.8746 \times 265.5}{(T_{sfc} - T_0 + 265.5)^2}, \quad (55)$$

These values are used to solve surface temperature T_{sfc} described below.

Snowfall W_{snow} is parameterized from precipitation W_{prcp} and surface air temperature T_a [16, 3]:

$$W_{snow} = \frac{\rho_f}{\rho_s} r_s W_{prcp}, \quad (56)$$

where

$$r_s = \begin{cases} 1.0 & (T_a - T_0 < -5) \\ 1.0 - (T_a - T_0 + 5) \times 0.1 & (-5 < T_a - T_0 < 5) \\ 0.0 & (T_a - T_0 > 5) \end{cases} \quad (57)$$

is the fraction of precipitation falling as snow. Snowfall contributes to snow growth over sea-ice and the remainder, rainfall $W_{rain} = (1 - r_s) W_{prcp}$, is treated as surface runoff flowing into the ocean.

5.2.2 Snow-Free Sea-Ice

If sea-ice is not covered with snow ($h_s = 0$), sea-ice surface temperature T_{sfc} is solved to satisfy the energy balance there (Fig. 3b).

A fraction I_0 of the net incident short-wave radiation, $(1 - \alpha_{sfc}) R_{SW} \downarrow$, penetrates the bare sea-ice. In order to parameterize this process within zero-layer thermodynamics model, some part of I_0 is assumed to be absorbed by sea-ice and used for surface heat budget, and remaining penetrates sea-ice. This penetration of short-wave radiation, $R_{SW}^p \downarrow$, is parameterized as [17, 3]:

$$R_{SW}^p \downarrow = I_0 (1 - \alpha_{sfc}) R_{SW} \downarrow \exp(-1.5 h_i) \quad (58)$$

where h_i is sea-ice thickness.

Conductive heat flux of sea-ice, $G_i \downarrow$, becomes

$$G_i \downarrow = \frac{k_i}{h_i} (T_{sfc} - T_{btm}), \quad (59)$$

where k_i is thermal conductivity of sea-ice, h_i sea-ice thickness, and $T_{btm} = T_w^{frz}$ sea-ice bottom temperature.

The energy balance at the sea-ice surface is

$$\Delta Q_{sfc} \equiv Q_{sfc} \downarrow - R_{SW}^p \downarrow - G_i \downarrow = 0, \quad (60)$$

and sea-ice surface temperature T_{sfc} is calculated iteratively using Newton-Raphson method (5 times) to maintain this energy balance:

$$\begin{aligned} \Delta Q_{sfc} [T_{sfc}^{(i+1)}] &\approx \Delta Q_{sfc} [T_{sfc}^{(i)}] \\ &+ \left. \frac{\partial \Delta Q_{sfc}}{\partial T_{sfc}} \right|_{T_{sfc}^{(i)}} (T_{sfc}^{(i+1)} - T_{sfc}^{(i)}) \\ &= 0, \end{aligned} \quad (61)$$

or sea-ice surface temperature is updated as

$$T_{sfc}^{(i+1)} = T_{sfc}^{(i)} - \Delta Q_{sfc} [T_{sfc}^{(i)}] / \left. \frac{\partial \Delta Q_{sfc}}{\partial T_{sfc}} \right|_{T_{sfc}^{(i)}}, \quad (62)$$

where $T_{sfc}^{(i)}$ is i -th iteration result and $\partial \Delta Q_{sfc} / \partial T_{sfc}$ is

$$\frac{\partial \Delta Q_{sfc}}{\partial T_{sfc}} \equiv \frac{\partial H_{lat} \downarrow}{\partial T_{sfc}} + \frac{\partial H_{sen} \downarrow}{\partial T_{sfc}} - 4\epsilon_{sfc} \sigma T_{sfc}^3 - \frac{k_i}{h_i}. \quad (63)$$

5.2.3 Snow-Covered Sea-Ice

When sea-ice is covered with snow ($h_s > 0$), snow surface temperature T_{sfc} is solved to satisfy the energy balances at the snow surface and at the snow/sea-ice interface (Fig. 3c).

In this case, no penetration of short-wave radiation is considered:

$$R_{SW}^p \downarrow = 0. \quad (64)$$

Conductive heat fluxes of snow, $G_s \downarrow$, and sea-ice, $G_i \downarrow$, become

$$G_s \downarrow = \frac{k_s}{h_s} (T_{sfc} - T_{ifc}), \quad (65)$$

$$G_i \downarrow = \frac{k_i}{h_i} (T_{ifc} - T_{btm}), \quad (66)$$

where k_s is thermal conductivity of snow, k_i thermal conductivity of sea-ice, h_s snow depth, h_i sea-ice thickness, T_{ifc} snow/sea-ice interface temperature, and $T_{btm} = T_w^{frz}$ sea-ice bottom temperature.

The energy balance at the snow surface is [6, Eq. (23)]

$$\Delta Q_{sfc} \equiv Q_{sfc} \downarrow - G_s \downarrow = 0, \quad (67)$$

and the energy balance at the snow/sea-ice interface is

$$\Delta Q_{ifc} \equiv G_s \downarrow - G_i \downarrow = 0. \quad (68)$$

From Eq. (68), interface temperature T_{ifc} is expressed as a function of snow surface temperature T_{sfc} as:

$$T_{ifc} = \frac{k_s h_i T_{sfc} + k_i h_s T_{btm}}{k_s h_i + k_i h_s}. \quad (69)$$

Therefore,

$$G_s \downarrow = G_i \downarrow = \frac{k_s k_i}{k_s h_i + k_i h_s} (T_{sfc} - T_{btm}). \quad (70)$$

Now ΔQ_{sfc} is a nonlinear function of T_{sfc} , and Eq. (67) is solved in the same way as for snow-free sea-ice, but in this case,

$$\begin{aligned} \frac{\partial \Delta Q_{sfc}}{\partial T_{sfc}} &\equiv \frac{\partial H_{lat} \downarrow}{\partial T_{sfc}} + \frac{\partial H_{sen} \downarrow}{\partial T_{sfc}} - 4\epsilon_{sfc} \sigma T_{sfc}^3 \\ &- \frac{k_s k_i}{k_s h_i + k_i h_s}. \end{aligned} \quad (71)$$

5.2.4 Growth Rate of Sea-Ice and Snow

Consider the case that sea-ice is covered with snow ($h_s > 0$). If the snow surface temperature T_{sfc} exceeds melting point of snow, T_s^{mlt} , then T_{sfc} is fixed to T_s^{mlt} and the residual of snow surface heat flux, $\Delta Q_{sfc} [T_s^{mlt}]$, is used for snow melting:

$$F_s^{sfc} = \min \left(0, \frac{\Delta Q_{sfc} [T_s^{mlt}]}{\rho_s L_{mlt}} \right), \quad (72)$$

where ρ_s is snow density and L_{mlt} latent heat of fusion.

If sea-ice is not covered with snow ($h_s = 0$) and the sea-ice surface temperature T_{sfc} exceeds melting point of sea-ice, T_i^{mlt} , then T_{sfc} is fixed to T_i^{mlt} and the residual of sea-ice surface heat flux, $\Delta Q_{sfc} [T_i^{mlt}]$, is used for sea-ice melting:

$$F_i^{sfc} = \min \left(0, \frac{\Delta Q_{sfc} [T_i^{mlt}]}{\rho_i L_{mlt}} \right), \quad (73)$$

where ρ_i is sea-ice density and L_{mlt} latent heat of fusion.

Growth rate of sea-ice thickness at the sea-ice bottom is calculated from energy imbalance there. When snow lies on sea-ice ($h_s > 0$), conductive heat flux of sea-ice, $G_i \downarrow$, is expressed as a function of surface temperature T_{sfc} as

$$G_i \downarrow = \frac{k_s k_i}{k_s h_i + k_i h_s} (T_{sfc} - T_{btm}), \quad (74)$$

where k_s and k_i are thermal conductivities of snow and sea-ice, respectively, and $T_{btm} = T_w^{frz}$ is sea-ice bottom temperature. This expression is valid even for the case of no snow ($h_s = 0$). Turbulent heat flux through ocean/sea-ice interface, $H_{iw\downarrow}$, is parameterized as [18, 3]:

$$H_{iw\downarrow} = \rho_w c_{pw} C_t (T_{btm} - T_w), \quad (75)$$

where ρ_w is seawater density, c_{pw} specific heat of seawater, C_t the bulk transfer coefficient (a namelist parameter with dimension of $m s^{-1}$), and T_w ocean surface temperature. At the sea-ice bottom, growth rate of sea-ice thickness, F_i^{btm} , is expressed as:

$$F_i^{btm} = -\frac{G_i\downarrow - H_{iw\downarrow}}{\rho_i L_{mli}}, \quad (76)$$

where ρ_i is sea-ice density and L_{mli} latent heat of fusion. Positive (negative) F_i^{btm} represents sea-ice formation (melting).

The aging process of snow is parameterized as a rate F_{s2i} at which snow is changed into ice [7]:

$$F_{s2i} = \gamma_s h_s + \frac{1}{\Delta t} \max\left(0, h_s - \frac{\rho_w - \rho_i}{\rho_s} h_i\right). \quad (77)$$

The first term represents an assumption that conversion of snow into ice simply depends on temporal scale $\gamma_s = 2.0 \times 10^{-7} s^{-1}$ and snow depth h_s . The second term expresses the case that accumulated snow suppress the sea-ice surface below the sea level.

Finally, growth rates of snow depth, F_s , and sea-ice thickness, F_i , at sea-ice region are calculated as follows:

$$F_s = F_s^{sc} - F_{s2i}, \quad (78)$$

$$F_i = F_i^{sc} + F_i^{btm} + \frac{\rho_s}{\rho_i} F_{s2i}. \quad (79)$$

5.3 Total Growth Rate of Sea-Ice and Snow

Growth rate of sea-ice thickness, F_i^{eff} , is expressed as a combination of growth rates at open ocean, F_w , and sea-ice region, F_i :

$$F_i^{eff} = (1 - A_i) F_w + A_i F_i. \quad (80)$$

Growth rate of snow depth, F_s^{eff} , is given as a sum of growth rate at sea-ice region, F_s , and snowfall W_{snw} minus sublimation $W_{sub} = -H_{lat\downarrow} / L_{sub}$:

$$F_s^{eff} = A_i (F_s + W_{snw} - W_{sub}). \quad (81)$$

Growth rate of sea-ice concentration, F_A , is

$$F_A = (1 - A_i) F_w / h_0 + A_i \min(0, F_i) / 2h_i^{eff}, \quad (82)$$

where $h_0 = 0.2$ m is cut off thickness between thick and thin ice.

6. Boundary Conditions for the Ocean Component

Finally, momentum flux τ_{surf} , short-wave radiation flux $Q_{SW\downarrow}$, total heat flux Q_{surf} , and fresh water flux W_{surf} at ocean surface are calculated in subroutine *giosbc* to drive ocean component of OIFES.

6.1 Momentum Flux

If there is no sea-ice, the momentum flux through the sea surface, τ_{surf} , is composed as [2, Eq. (4.32)]:

$$\tau_{surf} = \tau_{wind} + \tau_{fresh} \quad (83)$$

where τ_{wind} is the wind stress and τ_{fresh} represents momentum transfer in relation with a fresh water flux. This equation is extended to the region covered with sea-ice as:

$$\tau_{surf} = (1 - A_i) \tau_{aw} + A_i \tau_{iw} + \tau_{fresh} \quad (84)$$

where τ_{aw} is direct momentum input from the atmosphere and τ_{iw} the stress at ocean/sea-ice interface determined from sea-ice dynamics.

6.2 Heat Flux

Surface heat flux due to downward short-wave radiation, $Q_{SW\downarrow}$, is expressed as a combination of direct short-wave radiation flux at open ocean and penetrative flux below sea-ice (without snow cover):

$$Q_{SW\downarrow} = (1 - A_i) (1 - \alpha_w) R_{SW\downarrow} + A_i R_{SW\downarrow}^p, \quad (85)$$

where α_w is seawater albedo. Total heat flux Q_{surf} is

$$Q_{surf} = (1 - A_i) (Q_{aw} + H_{snw\downarrow}) + A_i (R_{SW\downarrow}^p + H_{iw\downarrow}), \quad (86)$$

where Q_{aw} is net heat flux between atmosphere and ocean (including short-wave radiation flux), $H_{snw\downarrow} = -\rho_s L_{mli} W_{snw}$ latent heat of snow melting³, and $H_{iw\downarrow}$ turbulent heat flux at sea-ice/ocean interface.

³ This process is considered only if the option *cfes* is enabled.

6.3 FreshWater Flux

Total fresh water flux W_{surf} is expressed as follows:

$$W_{surf} = (1 - A_i) (W_{prcp} - W_{evap}) + A_i (W_{rain} + W_{ice}) + W_{rivr}, \quad (87)$$

where $W_{prcp} = W_{rain} + W_{snw}$ is total precipitation, $W_{evap} = -H_{lat} \downarrow / \rho_w L_{vap}$ evaporation, W_{rain} sea-ice surface runoff due to rainfall, W_{ice} fresh water flux due to sea-ice formation/melting and snow melting, and W_{rivr} river runoff.

7. Code Optimization

Here, some issues on code optimization are described. Generally speaking, computational cost of a sea-ice component is much smaller than that of an ocean component in a coupled ocean–sea-ice model, because calculation of sea-ice is, at most, two-dimensional while calculation of ocean is three-dimensional. However, OFES has excellent computational efficiency for the Earth Simulator, so the sea-ice component of OIFES is carefully optimized not to drag down the total computational performance.

Source code of the sea-ice component is optimized in a similar manner applied to OFES. First of all, most of DO loops are vectorized in the zonal direction. This is an important work for vector computers like the Earth Simulator. Then, they are parallelized using MPI library such as MPI_SEND and MPI_RECV. We employ one-dimensional domain decomposition in the meridional direction as for OFES.

Table 4 shows results obtained from “flow trace analysis” on major subroutines relating to the sea-ice component for the case in which the horizontal resolution is 0.25° in both longitude and latitude. We used 45 computational nodes of the Earth Simulator with 360 MPI processes. Note that in this case the numbers of grid

points in the zonal and the meridional directions are 1440 and 720, respectively, and therefore, each MPI process treats 2 zonal strips as computational domain with 4 halo regions (2 for the northern side and 2 for the southern side). Execution times of these subroutines are 1.4% at most, and the total execution time of the sea-ice component is about 6%.⁴ Their vector operation ratios are about 99% and averaged vector lengths are about 240, which is close to the maximum value of 256. Some of them (*asflx*, *form*, and *budgets*) attain the flops values over 40% of the theoretical peak performance of 8 Gflops. On the other hand, subroutines *plast*, *ice_slow*, and *advdif* exhibit the low flops values, because the communication costs are relatively large in these subroutines, and *ice_slow* is the main driving routine for the sea-ice component.

8. Preliminary Results

In this section, some preliminary results on sea-ice obtained from a coupled atmosphere–ocean simulation using AFES and OIFES, namely CFES, are presented in order to show potential of our sea-ice model.

8.1 Setting of Simulation

Brief overview of a coupled simulation is as follows. Horizontal resolution of the ocean/sea-ice component is 0.25° in both longitude and latitude. It contains 54 levels in vertical and the top level has thickness of 5 m. Parameters relating to sea-ice are summarized in Table 3. Initial conditions of the ocean component are climatological temperature and salinity of the World Ocean Atlas 1998 [19, 20, 21, 22, 23, 24] with no motion. Model resolution of the atmospheric component is T106 (triangle truncation of wave number 106, $\sim 1.1^\circ$) in horizontal and 48 layers in vertical. Detailed model configurations may be presented in another report. Monthly-mean simulation results of the 3rd model year rather than climatological ones are shown below due to short of integration time.

Table 4 Results obtained from “flow trace analysis”.

Subroutine	Description	Exec. Time [%]	MFLOPS	V. Ratio [%]	V. Length
<i>plast</i>	strain rate and viscosity	1.4	741.3	98.56	240.6
<i>asflx</i>	air–sea flux	1.0	3303.1	99.60	240.9
<i>ice_slow</i>	main routine for sea-ice	0.8	44.7	92.59	223.3
<i>advdif</i>	advection and diffusion	0.7	467.7	98.03	238.1
<i>form</i>	momentum equation	0.6	3425.0	99.30	240.6
<i>budgets</i>	surface energy budget	0.6	3729.9	99.46	206.6
<i>elast</i>	elastic equation	0.5	2393.0	98.92	237.8

⁴ These values depend on a number of elastic subcycle, N_{evp} .

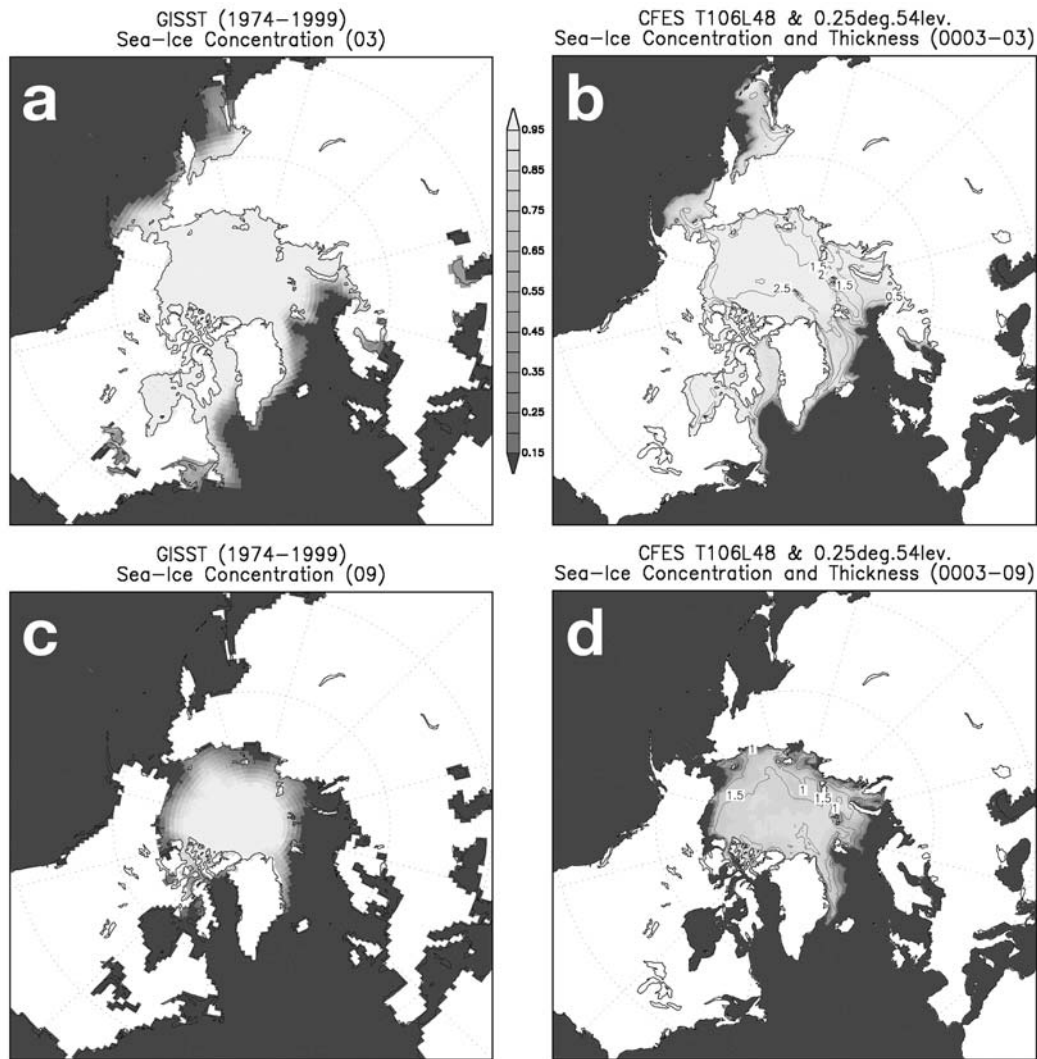


Fig. 4 (a) (c) Observed and (b) (d) simulated sea-ice concentration in the Arctic region. Effective sea-ice thickness is overplotted in (b) and (d). Contour interval is 0.5 m. (a) (b) March. (c) (d) September.

8.2 Arctic Region

Figure 4 shows comparison between observed and simulated sea-ice concentration in the Arctic region in March (Fig. 4a, b) and in September (Fig. 4c, d). Climatological monthly-mean observations are calculated using global sea-ice concentration data of GISST [25] from 1974 through 1999. Seasonal variation of simulated sea-ice extent well captures the observed feature such that a main portion of sea-ice remains throughout the year. Simulated effective sea-ice thickness is also shown in Fig. 4. Overall pattern that sea-ice is thicker on the Greenland side than on the Eurasian side is realistically reproduced, but the sea-ice thickness is about half of the typical observed value (3–5 m).

In Fig. 5, simulated sea-ice velocity in the Arctic Ocean is plotted. Two major structures, the Trans-Polar Drift on the Eurasian side of the Ocean and the Beaufort

Gyre in the Canada Basin, are well reproduced in March (Fig. 5a), while reversal of the Trans-Polar Drift in September (Fig. 5b) may be unrealistic.

8.3 Antarctic Region

Simulated sea-ice concentration in the Antarctic region is compared with climatological observation (GISST) in Fig. 6. In both seasons (February and August) they look similar. However, absence of sea-ice around the Antarctic coast in February should be pointed out as a noticeable problem. Simulated sea-ice thickness in winter (Fig. 6d) is acceptable.

Figure 7 shows simulated sea-ice velocity around the Antarctica. Clockwise circulations corresponding to the Weddell Gyre and the Ross Gyre are clearly seen in August (Fig. 7b).

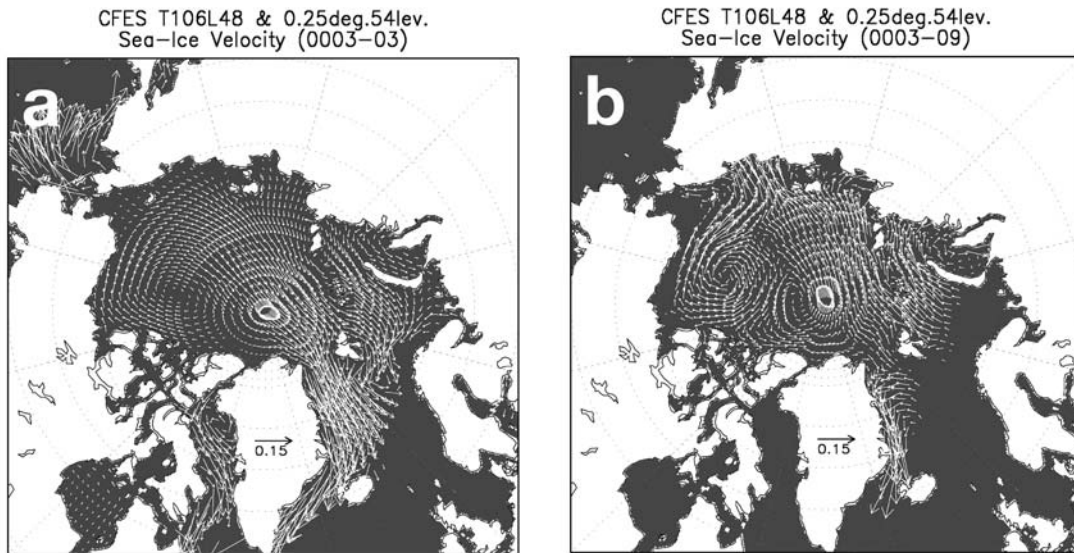


Fig. 5 Simulated sea-ice velocity [m s^{-1}] in the Arctic region. (a) March. (b) September.

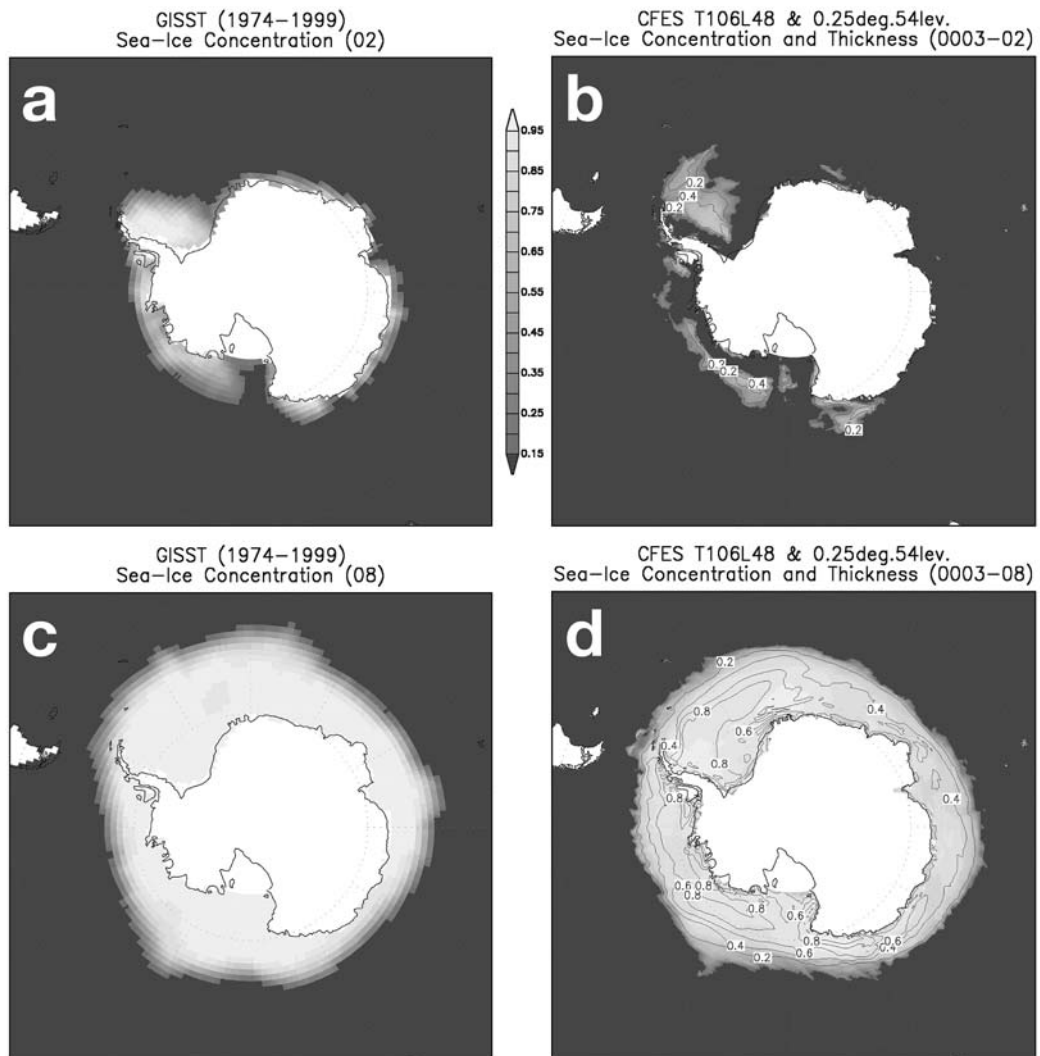


Fig. 6 Same as Fig. 4 but in the Antarctic region and contour interval is 0.2 m. (a) (b) February. (c) (d) August.

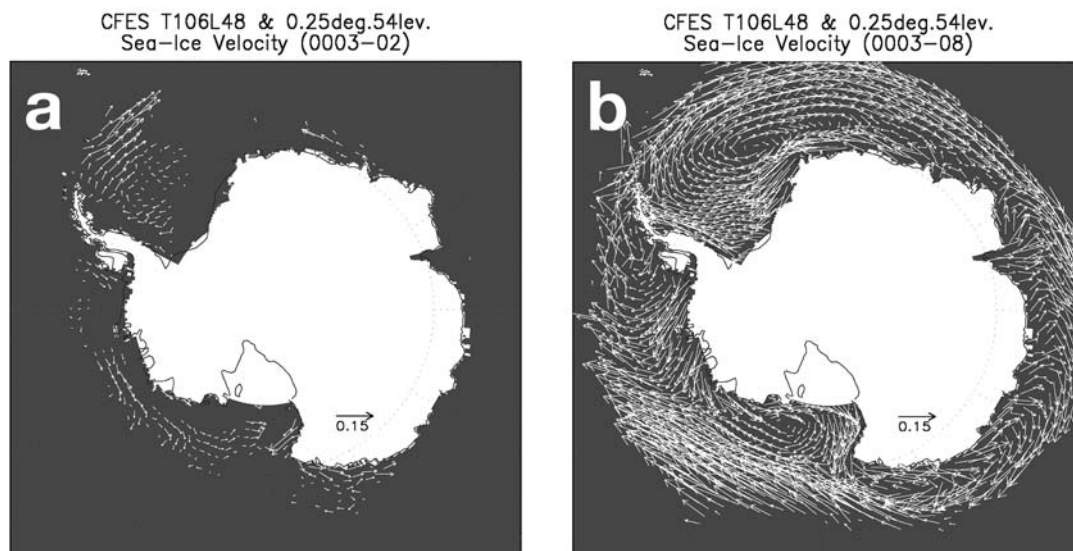


Fig. 7 Same as Fig. 5 but in the Antarctic region. (a) February. (b) August.

8.4 Short Summary

Our coupled ocean–sea-ice model, OIFES, seems to have the capability of simulating the global sea-ice variability: simulated sea-ice concentration, thickness, and velocity fields are fairly good in reproducing observed features in both the Arctic and the Antarctic regions and in both summer and winter. Some discrepancies found between observation and simulation may be reduced by making efforts at tuning model parameters of both ocean and sea-ice components, and longer model integration is necessary for detailed comparison with observation.

Acknowledgements

The authors would like to thank Prof. Moto Ikeda for his valuable advice and Dr. Toru Miyama for his significant contribution to improvement of OIFES. We also thank Messrs. Takashi Abe and Akira Azami for their help in optimizing the source code of OIFES. Development of OIFES is partly supported by MEXT (Ministry of Education, Culture, Sports, Science and Technology) RR2002 Project for Sustainable Co-existence of Human, Nature and the Earth, category 7 (PI: Prof. Toshiyuki Awaji).

(This article is reviewed by Dr. Tetsuya Sato.)

References

- [1] Y. Masumoto, H. Sasaki, T. Kagimoto, N. Komori, A. Ishida, Y. Sasai, T. Miyama, T. Motoi, H. Mitsudera, K. Takahashi, H. Sakuma, and T. Yamagata, A fifty-year eddy-resolving simulation of the world ocean: Preliminary outcomes of OFES (OGCM for the Earth Simulator), *J. Earth Simulator*, vol.1, pp.35–56, 2004.
- [2] R. C. Pacanowski, and S. M. Griffies, *MOM 3.0 Manual*, Geophysical Fluid Dynamics Laboratory/National Oceanic and Atmospheric Administration, Princeton, NJ, U.S.A., 680 pp, 2000.
- [3] X. Zhang, and J. Zhang, Heat and freshwater budgets and pathway in the Arctic Mediterranean in a coupled ocean sea-ice model, *J. Oceanogr.*, vol.57, no.2, pp.207–234, 2001.
- [4] R. C. Pacanowski, *MOM2 documentation, user's guide and reference manual*, Geophysical Fluid Dynamics Laboratory/National Oceanic and Atmospheric Administration, Princeton, NJ, U.S.A., 232 pp, 1995.
- [5] W. D. Hibler III, A dynamic thermodynamic sea ice model, *J. Phys. Oceanogr.*, vol.9, no.4, pp.815–846, 1979.
- [6] C. L. Parkinson, and W. M. Washington, A large scale numerical model of sea ice, *J. Geophys. Res.*, vol.84, no.C1, pp.311–337, 1979.
- [7] J. M. Oberhuber, D. M. Holland, and L. A. Mysak, A thermodynamic-dynamic snow sea-ice model, in *Ice in the Climate System*, W.R. Peltier (Ed.), NATO ASI Series, Series I: Global Environmental Change, pp.653–673, 1993.
- [8] E. C. Hunke, and J. K. Dukowicz, An elastic–viscous–plastic model for sea ice dynamics, *J. Phys. Oceanogr.*, vol.27, no.9, pp.1849–1867, 1997.
- [9] E. C. Hunke, and J. K. Dukowicz, The elastic–viscous–plastic sea ice dynamics model in general orthogonal curvilinear coordinates on a sphere—Incorporation of metric terms, *Mon. Wea. Rev.*, vol.130, no.7, pp.1848–1865, 2002.
- [10] W. Ohfuchi, H. Nakamura, M. K. Yoshioka, T. Enomoto, K. Takaya, X. Peng, S. Yamane, T. Nishimura, Y. Kurihara, and K. Ninomiya, 10-km mesh meso-scale

- resolving simulations of the global atmosphere on the Earth Simulator: Preliminary outcomes of AFES (AGCM for the Earth Simulator), *J. Earth Simulator*, vol.1, pp.8–34, 2004.
- [11] G. L. Mellor, and L. Kantha, An ice-ocean coupled model, *J. Geophys. Res.*, vol.94, no.C8, pp.10,937–10,954, 1989.
- [12] J. Zhang, and W. D. Hibler III, On an efficient numerical method for modeling sea ice dynamics, *J. Geophys. Res.*, vol.102, no.C4, pp.8691–8702, 1997.
- [13] A. J. Semtner Jr., A model for the thermodynamic growth of sea ice in numerical investigations of climate, *J. Phys. Oceanogr.*, vol.6, no.3, pp.379–389, 1976.
- [14] W. G. Large, and S. Pond, Open ocean momentum flux measurements in moderate to strong winds, *J. Phys. Oceanogr.*, vol.11, no.3, pp.324–336, 1981.
- [15] W. G. Large, and S. Pond, Sensible and latent heat flux measurements over the oceans, *J. Phys. Oceanogr.*, vol.12, no.5, pp.464–482, 1982.
- [16] J. W. Weatherly, and J. E. Walsh, The effects of precipitation and river runoff in a coupled ice-ocean model of the Arctic, *Clim. Dyn.*, vol.12, no.11, pp.785–798, 1996.
- [17] T. C. Grenfell, and G. A. Maykut, The optical properties of ice and snow in the Arctic Basin, *J. Glaciol.*, vol.18, no.80, pp.445–463, 1977.
- [18] E. E. Ebert, and J. A. Curry, An intermediate one-dimensional thermodynamic sea ice model for investigating ice-atmosphere interactions, *J. Geophys. Res.*, vol.98, no.C6, pp.10,085–10,109, 1993.
- [19] J. I. Antonov, S. Levitus, T. P. Boyer, M. E. Conkright, T. O'Brien, and C. Stephens, *World Ocean Atlas 1998 Vol. 1: Temperature of the Atlantic Ocean*, NOAA Atlas NESDIS 27. U.S. Government Printing Office, Washington, D.C., 1998a.
- [20] J. I. Antonov, S. Levitus, T. P. Boyer, M. E. Conkright, T. O'Brien, and C. Stephens, *World Ocean Atlas 1998 Vol. 2: Temperature of the Pacific Ocean*, NOAA Atlas NESDIS 28. U.S. Government Printing Office, Washington, D.C., 1998b.
- [21] J. I. Antonov, S. Levitus, T. P. Boyer, M. E. Conkright, T. O'Brien, C. Stephens, and B. Trotsenko, *World Ocean Atlas 1998 Vol. 3: Temperature of the Indian Ocean*, NOAA Atlas NESDIS 29. U.S. Government Printing Office, Washington, D.C., 1998c.
- [22] T. P. Boyer, S. Levitus, J. I. Antonov, M. E. Conkright, T. O'Brien, and C. Stephens, *World Ocean Atlas 1998 Vol. 4: Salinity of the Atlantic Ocean*, NOAA Atlas NESDIS 30. U.S. Government Printing Office, Washington, D.C., 1998a.
- [23] T. P. Boyer, S. Levitus, J. I. Antonov, M. E. Conkright, T. O'Brien, and C. Stephens, *World Ocean Atlas 1998 Vol. 5: Salinity of the Pacific Ocean*, NOAA Atlas NESDIS 31. U.S. Government Printing Office, Washington, D.C., 1998b.
- [24] T. P. Boyer, S. Levitus, J. I. Antonov, M. E. Conkright, T. O'Brien, C. Stephens, and B. Trotsenko, *World Ocean Atlas 1998 Vol. 6: Salinity of the Indian Ocean*, NOAA Atlas NESDIS 32. U.S. Government Printing Office, Washington, D.C., 1998c.
- [25] E. Parker, M. Jackson, and E. B. Horton, The 1961–1990 GISST2.2 sea surface temperature and sea ice climatology, *Climate Research Technical Note*, no.63, Hadley Centre, UK Met Office, Bracknell, UK, 1995.